

# Generative Networks for Precision Enthusiasts

Anja Butter<sup>1</sup>, Theo Heimel<sup>1</sup>, Sander Hummerich<sup>1</sup>, Tobias Krebs<sup>1</sup>,  
Tilman Plehn<sup>1</sup>, Armand Rousselot<sup>2</sup>, and Sophia Vent<sup>1</sup>

<sup>1</sup> Institut für Theoretische Physik, Universität Heidelberg, Germany

<sup>2</sup> Heidelberg Collaboratory for Image Processing, Universität Heidelberg, Germany

March 21, 2022

## Abstract

Generative networks are opening new avenues in fast event generation for the LHC. We show how generative flow networks can reach percent-level precision for kinematic distributions, how they can be trained jointly with a discriminator, and how this discriminator improves the generation. Our joint training relies on a novel coupling of the two networks which does not require a Nash equilibrium. We then estimate the generation uncertainties through a Bayesian network setup and through conditional data augmentation, while the discriminator ensures that there are no systematic inconsistencies compared to the training data.

---

## Content

<b>1</b>	<b>Introduction</b>	<b>2</b>
<b>2</b>	<b>Precision generator</b>	<b>2</b>
2.1	Data set	3
2.2	INN generator	4
<b>3</b>	<b>DiscFlow generator</b>	<b>9</b>
3.1	Discriminator reweighting	9
3.2	Joint training	11
<b>4</b>	<b>Uncertainties and control</b>	<b>15</b>
4.1	Bayesian network	15
4.2	Conditional augmentations	19
4.3	Discriminator for consistency	20
<b>5</b>	<b>Outlook</b>	<b>20</b>
	<b>References</b>	<b>22</b>

---

## 1 Introduction

Precise first-principle simulations provided by the theory community are a defining feature of LHC physics. They are based on perturbative quantum field theory with fundamental Lagrangians as their physics input, and they provide the simulated events necessary for modern LHC analyses and inference. Because of the close correlation of complexity and precision in perturbative calculations, precision and speed are, largely, two sides of the same medal. Both of these sides are facing major challenges for the LHC Runs 3 and 4, and the hope is that machine learning and its modern numerics toolbox allow us to provide the simulations needed for a 25-fold increase of LHC data as compared to Run 2.

In recent years, modern machine learning has shown great potential to improve LHC simulations [1]. Underlying techniques include GANs [2–4], VAEs [5, 6], normalizing flows [7–11], and their invertible network (INN) variant [12–14]. As part of the standard LHC simulation chain, modern neural networks can be applied to the full range of phase space integration [15, 16], phase space sampling [17–20], amplitude computations [21, 22], event subtraction [23], event unweighting [24, 25], parton showering [26–30], or super-resolution enhancement [31, 32]. In essence, there is no aspect of the standard event generation chain that cannot be improved through modern machine learning.

Conceptionally new developments are, for instance, based on fully NN-based event generators [33–37] or detector simulations [38–48]. Unlike forward Monte Carlo simulations, these network generators can be inverted. Conditional GANs and INNs allow us to invert the simulation chain to unfold detector effects [49, 50] and extract the hard scattering process at parton level in a statistically consistent manner [51]. Because of their superior statistical properties, the same conditional INNs can be used for simulation-based inference based on high-dimensional and low-level data [52]. Finally, normalizing-flow or INN generators provide new opportunities when we combine them with Bayesian network concepts [53–58] to construct uncertainty-controlled generative networks [59].

In this paper we combine the full range of ML-concepts to build an NN-based LHC event generator which meets the requirements in terms of phase space coverage, precision, and control of different uncertainties. We first present a precision INN generator in Sec. 2 which learns underlying phase space densities such that kinematic distributions are reproduced at the percent level, consistent with the statistical limitations of the training data. Next, our inspiration by GANs leads us to construct the DiscFlow discriminator–generator architecture to control the consistency of training data and generative network in in Sec. 3. Finally, in Sec. 4 we illustrate three ways to control the network training and estimate remaining uncertainties (i) through a Bayesian generative network, (ii) using conditional augmentations for systematic or theory uncertainties, and (iii) using the DiscFlow discriminator for controlled reweighting. While we employ forward event generation to illustrate these different concepts, our results can be directly transferred to inverted simulation, unfolding, or inference problems.

## 2 Precision generator

As we will show in this paper, generative networks using normalizing flows have significant advantages over other network architectures, including GANs, when it comes to LHC event generation. As a starting point, we show how flow-based invertible networks can be trained to generate events and reproduce phase space densities with high precision. Our network

architecture accounts for the complication of a variable number of particles in the final state.

## 2.1 Data set

The kind of NN-generators we discuss in this paper are trained on unweighted events at the hadronization level. We exclude detector effects because they soften sharp phase space features, so simulations without them tend to be more challenging and their results are more interesting from a technical perspective. The production of leptonically decaying  $Z$ -bosons with a variable number of jets is the ideal benchmark process. First, the network has to learn an extremely sharp  $Z$ -resonance peak. Second, QCD forces us to apply a geometric separation between jets, inducing a non-trivial topology of phase space. Finally, again because of QCD it does not make sense to define final states with a fixed number of jets, so our generative network has to cover a final state with a variable number of dimensions. Given these considerations we work with the process

$$pp \rightarrow Z_{\mu\mu} + \{1, 2, 3\} \text{ jets} , \quad (1)$$

simulated with SHERPA2.2.10 [60] at 13 TeV. We use CKKW merging [61] to generate a merged sample with up to three hard jets including ISR, parton shower, and hadronization, but no pile-up. The final state of the training sample is defined by FASTJET3.3.4 [62] in terms of anti- $k_T$  jets [63] with

$$p_{T,j} > 20 \text{ GeV} \quad \text{and} \quad \Delta R_{jj} > R_{\min} = 0.4 . \quad (2)$$

The jets and muons are ordered in  $p_T$ . Because jets have a finite invariant mass, our final state dimensionality is three for each muon plus four degrees of freedom per jet, giving us phase space dimensionalities 10, 14, and 18. Momentum conservation does not further reduce the dimensionality, as not every generated hadron is captured by the three leading jets. However, we will reduce this dimensionality by one by removing the symmetry on the choice of global azimuthal angle. Our combined sample size is 5.4M events, divided into 4.0M one-jet events, 1.1M two-jet events, and 300k three-jet events. This different training statistics will be discussed in more detail in Sec. 4.1.

To define a representation which makes it easier for an INN to learn the kinematic patterns we apply a standard pre-processing. First, each particle is represented by

$$\{ p_T, \eta, \phi, m \} . \quad (3)$$

Because we can extract a global threshold in the jet  $p_T$  we represent the events in terms of the variable  $\tilde{p}_T = \log(p_T - p_{T,\min})$ . This form leads to an approximately Gaussian distribution, matching the Gaussian latent-space distribution of the INN. Second, the choice of the global azimuthal angle is a symmetry of LHC events, so we instead train on azimuthal angles relative to the muon with larger transverse momentum in the range  $\Delta\phi \in [-\pi, \pi]$ . A transformation into  $\widetilde{\Delta\phi} = \text{atanh}(\Delta\phi/\pi)$  again leads to an approximately Gaussian distribution. For all phase space variables  $q$  we apply a centralization and normalization step

$$\tilde{q}_i = \frac{q_i - \overline{q_i}}{\sigma(q_i)} . \quad (4)$$

Finally, we apply a whitening/PCA transformation separately for each jet multiplicity.

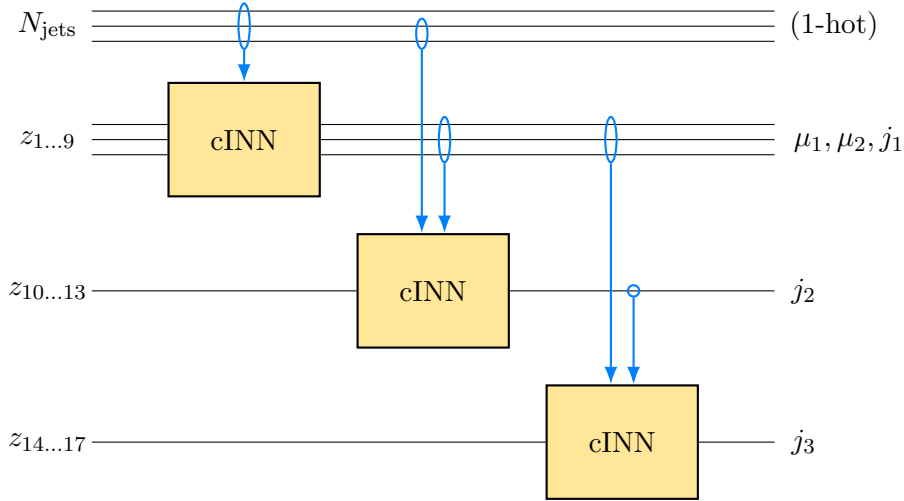


Figure 1: Generative flow architecture for events with two muons and one to three jets. The INNs relate the latent space (left) to the physical phase space (right).

## 2.2 INN generator

For a fixed final-state dimensionality we can use a completely standard INN [12, 59] to generate LHC events, especially after the preprocessing step defined above. Our technical challenge is to expand the INN architecture to generate final states with 9, 13, and 17 phase space dimensions. Of course, we could just split the training sample into different multiplicities and train a set of individual networks. However, in this case each of these networks has to learn the basic QCD patterns, making this naive approach inefficient and unstable.

To increase the efficiency, we stick to the same network for the common  $\mu_{1,2}$  and  $j_1$  momenta and add small additional networks for each additional jet, as illustrated in Fig. 1. Because the basic kinematic of the muons and the first jet does depend on possible additional jets, the base network gets the one-hot encoded number of jets as condition. Each of the additional networks is conditioned on the training observables of the previous networks and on the number of jets. Because the  $\mu\mu j$  and  $\mu\mu j j$  networks are trained on

hyperparameter	INN (Sec. 2.2)	INN (Sec. 3.1)	DiscFlow (Sec. 3.2)	BINN (Sec. 4.1)
LR scheduling	one-cycle	same	same	same
Starter LR	$10^{-4}$	$4 \cdot 10^{-4}$	$2 \cdot 10^{-4}$	$10^{-5}$
Maximum LR	$10^{-3}$	$4 \cdot 10^{-3}$	$2 \cdot 10^{-3}$	$10^{-4}$
Epochs	100	200	200	100
Batch size	1024	2048	2048	3072
ADAM $\beta_1, \beta_2$	0.9, 0.99	0.9, 0.99	0.5, 0.9	same
Coupling block	cubic spline	same	same	same
# spline bins	60	same	same	same
# coupling blocks	25	25	25	20
Layers per block	3	3	3	6
# generated events	2M	2M	2M	1M

Table 1: Training setup and hyperparameters for the INN generators used in our different setups.

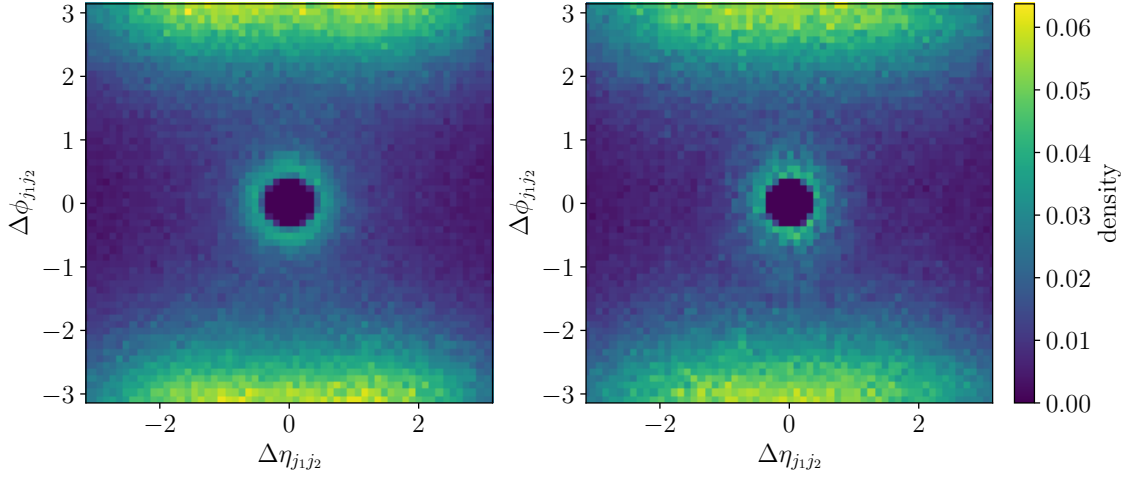


Figure 2: Jet-jet correlations for events with two jets. We show truth (left) and INN-generated events (right).

events with mixed multiplicities, we guarantee a balanced training by drawing a random subset of the training data set at the beginning of each epoch containing equal numbers of events from all different multiplicities. While all three networks are trained separately, they are combined as a generator.

Our network is implemented using PYTORCH [64] with the ADAM optimizer [65], and a one-cycle learning-rate scheduler [66]. The affine coupling blocks of the standard conditional INN setup [51, 67] are replaced by cubic spline coupling blocks [68], which are more efficient in learning complex phase space patterns precisely and reliably. The coupling block splits the target space into bins of variable width based on trainable support points, which are connected with a cubic function. They are combined with random but fixed rotations to ensure interaction between all input variables. The parameter ranges of input, output and intermediate spaces are limited to  $[-10, 10]$  on both sides of the coupling blocks, numbers outside this range are mapped onto themselves. The individual coupling blocks split their input vector in two halves  $(u_i, v_i)$  and transforms  $v_i$  as

$$v_i' = s(v_i; \chi(u_i, c_i)) . \quad (5)$$

The  $c_i$  are the conditional inputs of the network. The function  $\chi$  is a fully connected sub-network with  $2n_{\text{bins}} + 2$  outputs, where  $n_{\text{bins}}$  is the number of spline bins. They encode the horizontal and vertical positions of the spline knots and its slope at the boundaries. The loss function for a cINN  $\psi$  with a batch of  $B$  inputs  $x_i$  and conditions  $c_i$ , resulting in Jacobians  $J_i$ , is then given by

$$\mathcal{L}_G = \sum_{i=1}^B \left( \frac{\psi(x_i; c_i)^2}{2} - \log J_i \right) . \quad (6)$$

in order to ensure a Gaussian latent space distribution. We list all hyperparameters in Tab. 1.

### Magic transformation

A major challenge of the  $Z + \text{jets}$  final state is illustrated in Fig. 2, where we show the  $\Delta\phi$  vs  $\Delta\eta$  correlations for the exclusive 2-jet sample. We see that most events prefer a

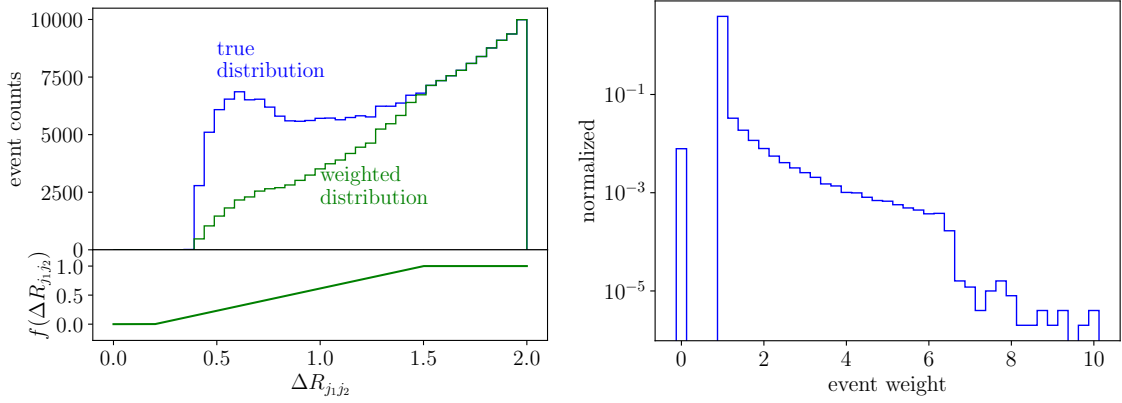


Figure 3: Left:  $\Delta R_{j1,j2}$ -distribution for  $Z+2$  jets events before and after the transformation of Eq.(8). Right: histogram of the weights of the generated events.

back-to-back topology, but a small number of events features two jets recoiling against the  $Z$ , cut off by the requirement  $\Delta R_{jj} > 0.4$ . The ring around the corresponding small circle is a local maximum, and inside the ring the phase space density drops to zero. Because this entire structure lives in a poorly populated phase space region, the INN typically ignores the local maximum and smoothly interpolates over the entire ring-hole structure. We emphasize that in our case this is not a problem with the non-trivial phase space topology [69], because the network is able to interpolate smoothly through these holes, but a problem of the precision with which the network learns features just around these holes.

To map out the local maximum structure we make use of the fact that our network is extremely efficient at interpolating smooth functions. To exploit this property we define a  $\Delta R_{jj}$ -dependent transformation which turns the actual phase space pattern into a smoothly dropping curve, let the network learn this smooth function extremely well, and then undo the transformation to re-build the local maximum pattern. A simple smoothing function for our case is

$$f(\Delta R) = \begin{cases} 0 & \text{for } \Delta R < R_- \\ \frac{\Delta R - R_-}{R_+ - R_-} & \text{for } \Delta R \in [R_-, R_+] \\ 1 & \text{for } \Delta R > R_+ \end{cases} \quad (7)$$

The transition region is defined such that it includes the cutoff to ensure non-vanishing weights,  $R_- < R_{\min} = 0.4$ , and its upper boundary is in a stable phase space regime. In our case we use  $R_- = 0.2$  and  $R_+ = 1.5$  without much fine-tuning. We also apply this transformation to the 3-jet sample, where all  $\Delta R_{jj}$ -distribution have similar challenges, through additional event weights

$$\begin{aligned} w^{(1\text{-jet})} &= 1 \\ w^{(2\text{-jet})} &= f(\Delta R_{j1,j2}) \\ w^{(3\text{-jet})} &= f(\Delta R_{j1,j2})f(\Delta R_{j2,j3})f(\Delta R_{j1,j3}) \end{aligned} \quad (8)$$

After training the INN generator on these modified events we also enforce the jet separation and set all event weights with  $\Delta R_{jj} < \Delta R_{\min}$  to zero. The inverse factor compensating

for our magic transformation is then

$$\tilde{f}(\Delta R) = \begin{cases} 0 & \text{for } \Delta R < R_{\min} \\ \frac{R_+ - R_-}{\Delta R - R_-} & \text{for } \Delta R \in [R_{\min}, R_+] \\ 1 & \text{for } \Delta R > R_+ \end{cases} . \quad (9)$$

To train the INN generator on weighted data the loss function of Eq.(6) has to be changed to

$$\mathcal{L}_G = \sum_{i=1}^B \left( \frac{\psi(x_i; c_i)}{2} - J(x_i) \right) \frac{w(x_i)}{\sum_{i=1}^B w(x_i)} , \quad (10)$$

per batch with size  $B$ . Here, the weights are defined in Eq.(8),  $x_i$  are the latent space vectors, and  $J_i$  are the corresponding logarithms of the Jacobian. In the right panel of Fig. 2 we see that our network architecture indeed captures the intricate structure in the jet-jet correlations. The distribution of the resulting event weights is shown in Fig. 3. By construction all finite event weights are above one, and hardly any of them reach values for more than seven, which implies that these weights can be easily removed by standard reweighting techniques.

Our magic transformation is similar to a refinement, defined as per-event modifications of phase space distributions [70], whereas reweighting uses weights for individual phase space points or events to improve the agreement between generator output and truth [71]. However, our transformation is, by standard phase-space mapping arguments, counter-intuitive\*. Instead of removing a leading dependence from a curve and learning a small but non-trivial difference, we smooth out a subtle pattern and rely on an outstanding network interpolation to learn the smoothed-out function better than the original pattern. This is motivated by the way flow networks learn distributions, which is more similar to a fit than a combination of local patterns [59]. The technical disadvantage of the smoothing transformation is that the generated events are now weighted, its advantage is that it is very versatile.

### INN-generator benchmark

In Fig. 4 we show a set of kinematic distributions for our training data, truth defined as a statistically independent version of the training sample, and the output of the INN-generator with the magic transformation of Eq.(8). We show distributions for exclusive  $Z + \{1, 2, 3\}$  jets samples and define the relative deviation for binned kinematic distributions as

$$\delta[\%] = 100 \frac{|\text{Model} - \text{Truth}|}{\text{Truth}} . \quad (11)$$

In the top row the final state consists of the  $Z$ -decay products and one recoil jet, and we see that the recoil spectrum as well as the sharp  $Z$ -mass are learned with high precision. That remains true when we add a second jet, including the critical  $\Delta R_{j_1 j_2}$  correlation discussed above. Finally, adding yet another jet the network learns the complete set of angular jet-jet correlations. Looking at the precision of the training sample, which consists of half of our full data set, we see that at least in the bulk of the kinematic distribution,

---

\*As a matter of fact, our magic transformation of the density is the exact opposite of the standard phase space mapping for Monte Carlo integration.

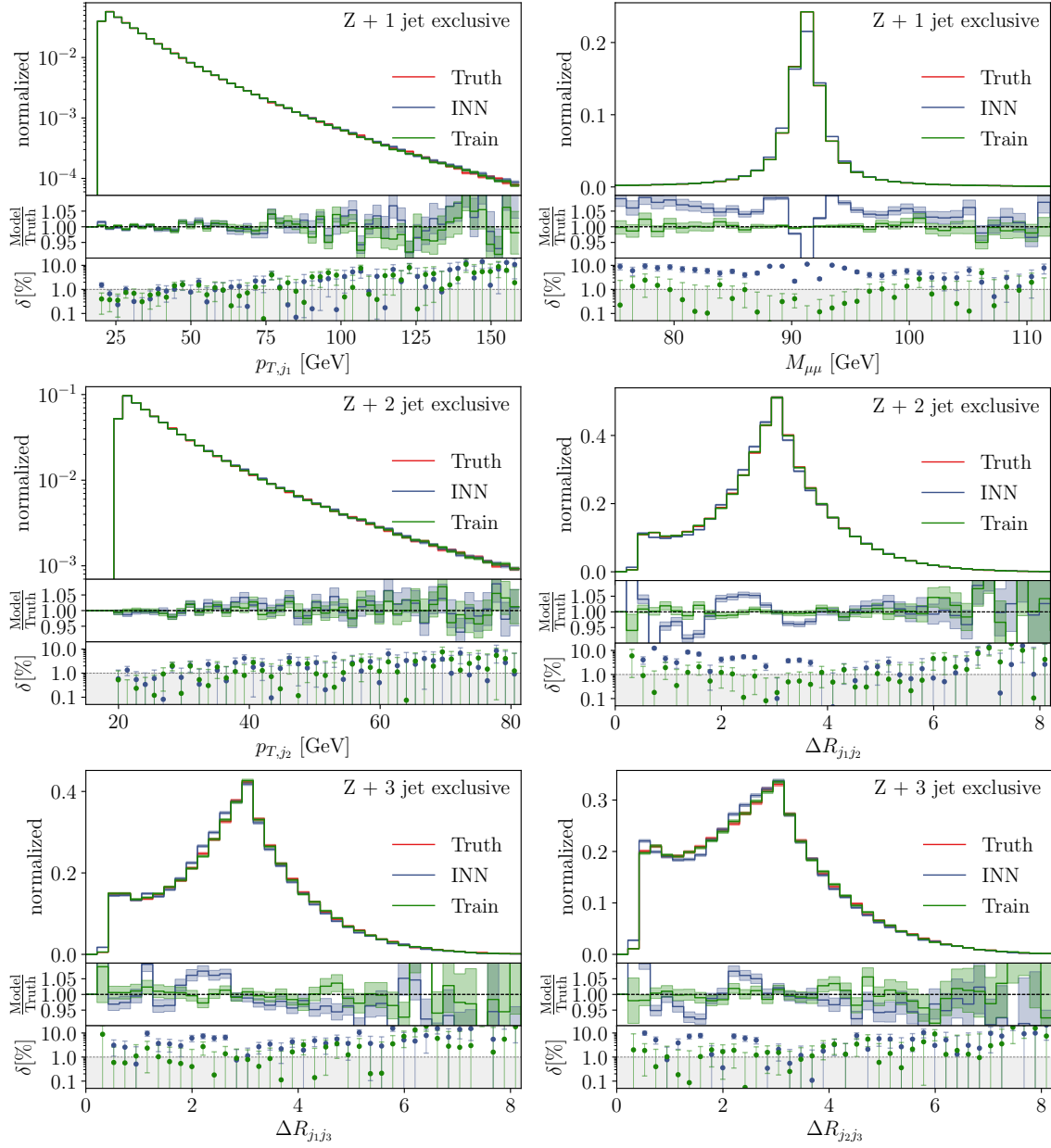


Figure 4: INN distributions for  $Z + 1$  jet (upper),  $Z + 2$  jets (middle), and  $Z + 3$  jets (lower) from a combined  $Z + \text{jets}$  generation. We show weighted events using the magic transformation of Eq.(8) to improve the  $\Delta R$  distributions.

the training data set agrees with truth at the percent level or better. This changes in the kinematic tails, where the statistical precision of the training data drops continuously. The level of agreement between the INN-generated events and truth also reaches the percent level in densely populated phase space regions, but it is slightly worse than the precision of the training sample. Also the  $Z$ -peak even in the 1-jet sample is not perfectly learned by the INN, which leaves us a little bit of work to do on the precision side.

### 3 DiscFlow generator

One way to systemically improve and control a precision INN-generator is to combine it with a discriminator. It is inspired by incredibly successful GAN applications also in LHC simulations [3,4,72]. In our preliminary studies we never reached a sufficient precision with established GAN architectures [36], while INN-generators proved very promising [59]. Compared to reweighting and refinement methods, a GAN-like setup has the advantage that the generator and discriminator networks already communicate during the joint training. We will show how such a discriminator network can be used to improve precision event generation and then show how a discriminator can be coupled to our INN generator in a new DiscFlow architecture.

#### 3.1 Discriminator reweighting

Before we train our INN-generator jointly with a discriminator, we illustrate the power of such a discriminator by training it independently and reweighting events with the discriminator output [71]. This requires that our discriminator output can eventually be transformed into a probabilistic correction. We train a simple network described in Tab. 2 by minimizing the cross entropy to extract a probability  $D(x_i) \rightarrow 0(1)$  for an identified generator (truth) event  $x_i$ . For a perfect generated sample the discriminator cannot tell generated events from true events, and the output becomes  $D(x_i) = 0.5$  everywhere. Using this discriminator output we define the event weight

$$w_D(x_i) = \frac{D(x_i)}{1 - D(x_i)} . \quad (12)$$

It corresponds to the ratio of true over generated phase space densities, so we can reweight each event to reproduce true kinematic distributions at the level they are encoded in the discriminator.

To see how precisely this kind of discriminator works we use the standard INN generator from Sec. 2.2. We omit the magic transformation described in Eq.(8), to define a challenge for the discriminator. For each jet-multiplicity of the cINN model, we train a discriminative model in parallel to the generative model, but for now without the two networks communicating with each other. The input to the three distinct discriminator networks, one per multiplicity, are the usual observables  $p_T, \eta, \phi$ , and  $m$  of Eq.(3) for each final-state particle. We explicitly include a set of correlations known to challenge our naive

hyper-parameter	value
LR scheduling	Reduce-on-plateau
Starter LR	$1 \cdot 10^{-2}$
Epochs	200
Batch size	2048
Adam $\beta_1, \beta_2$	0.5, 0.9
Layer type	Dense
Number layers	8
Internal size	256

Table 2: Training setup and hyperparameters for the discriminator.

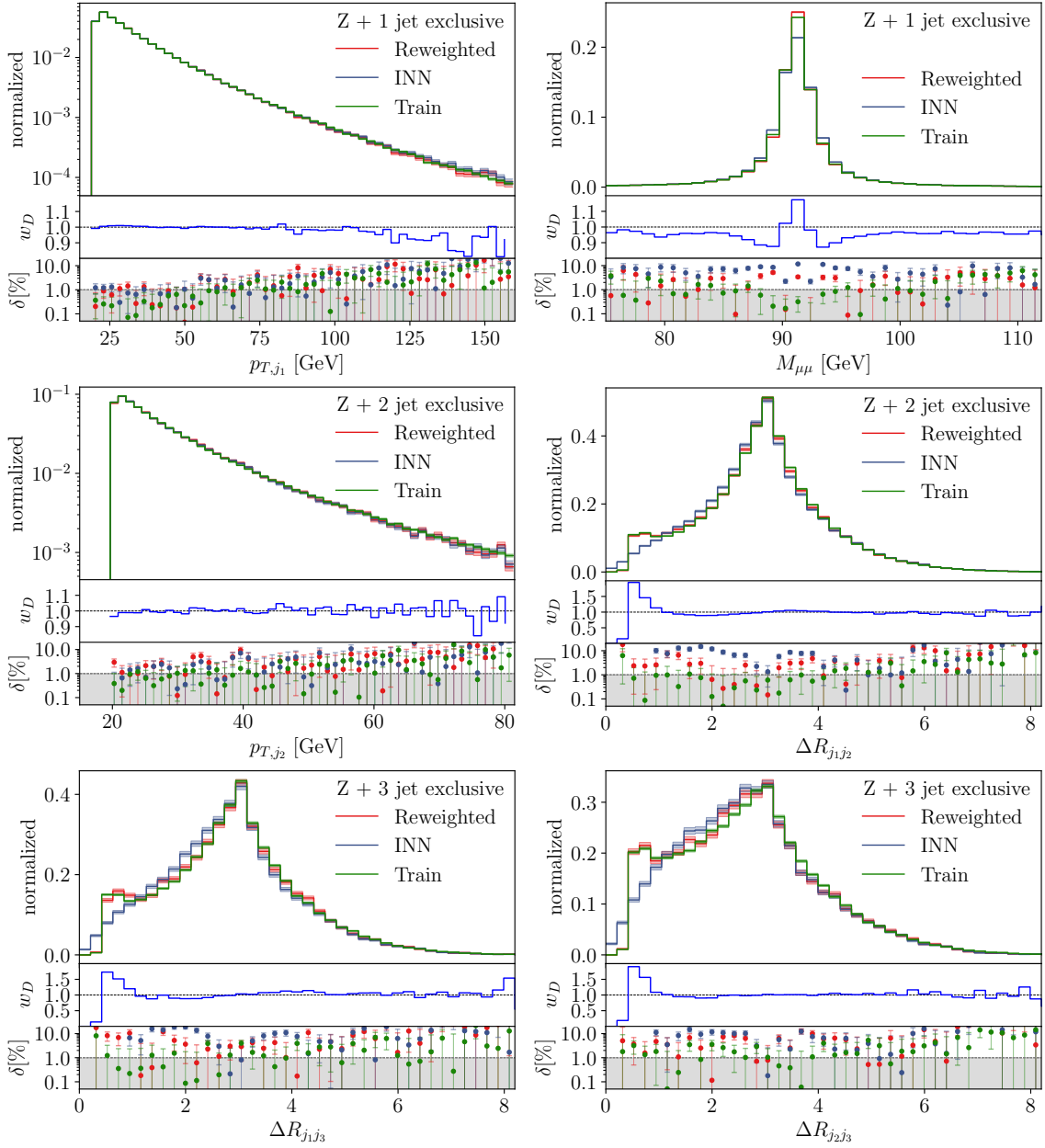


Figure 5: Discriminator-reweighted INN distributions for  $Z + 1$  jet (upper),  $Z + 2$  jets (middle), and  $Z + 3$  jets (lower) from a combined  $Z +$  jets generation. The bottom panels show the average correction factor obtained from the discriminator output, the INN results without reweighting are the same as in Fig. 4, except for slightly longer training.

INN generator and train the discriminator

$$\mathcal{L}_D = - \sum_i^B \log(1 - D(x_i)) - \sum_i^B \log(D(y_i)) \quad (13)$$

with generated vectors extended depending on the jet multiplicity

$$x_i = \{p_{T,j}, \eta_j, \phi_j, M_j\} \cup \{M_{\mu\mu}\} \cup \{\Delta R_{2,3}\} \cup \{\Delta R_{2,4}, \Delta R_{3,4}\}. \quad (14)$$

and corresponding training vectors  $y_i$ .

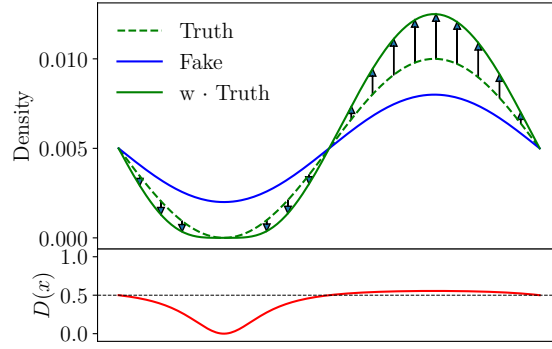


Figure 6: Illustration of the DiscFlow method. Weights computed by the discriminator shift the reference (true) density downwards whenever the generator (fake) distribution overshoots and vice-versa. This way the deviations of the to-be-trained generator density are over-exaggerated.

In Fig. 5 we show sample kinematic distributions for the  $Z + \{1, 2, 3\}$  jet final states. Truth is defined as the high-statistics limit of the training data. The INN events are generated with the default generator, without the magic transformation of Eq.(8), so they are unweighted events. The reweighted events are post-processed INN events with the average weight per bin shown in the second panel. While for some of the shown distribution a flat dependence  $w_D = 1$  indicates that the generator has learned to reproduce the training data to the best knowledge of the discriminator, our more challenging distributions are significantly improved by the discriminator. That includes the reconstructed  $Z$ -mass as well as the different  $\Delta R_{jj}$ -distributions.

Comparing the discriminator-reweighted performance to the magic transformation results in Fig. 4 we see that especially distributions like  $\Delta R_{j_1 j_2}$  or  $\Delta R_{j_1 j_3}$  are both reproduced extremely well. For the comparably flat  $p_T$ -distributions the precision of the reweighted events is becoming comparable to the training statistics, both for the bulk of the distribution and for the sparsely populated tails. Of all kinematic distributions we checked, the vector sum of all hard transverse momenta of the 5-jet final state is the only distribution where the naive INN-generator only learns the phase space distribution only at the 10% level. Also those are corrected fine by the discriminator reweighting.

While the discriminator reweighting provides us with an architecture that learns complex LHC events at the percent level or at the level of the training statistics, it comes with the disadvantage of generating weighted events and does not use the opportunity for the generator and discriminator to improve each other. Both of these open questions will be discussed in the next architecture.

### 3.2 Joint training

After observing the benefits from an additional discriminator network, the question is how we can make use of this second network most efficiently. If it is possible to train the discriminator and generator network in parallel and give them access to each other, a joint GAN-like setup could be very efficient [73]. Unfortunately, we have not been able to reach the required Nash equilibrium in an adversarial training for our specific INN setup. Instead, one of the two players was always able to overpower the other.

Instead of relying on a Nash equilibrium between the two competing network archi-

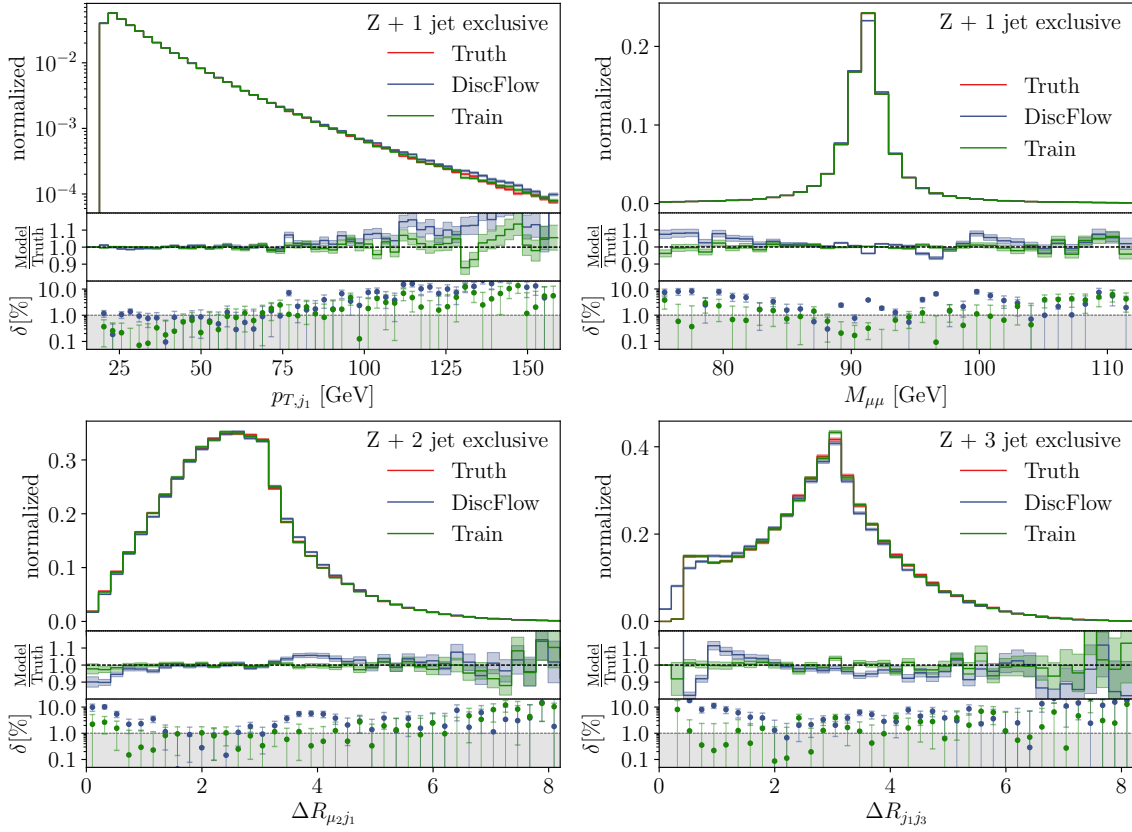


Figure 7: DiscFlow distributions for  $Z + 1$  jet,  $Z + 2$  jets, and  $Z + 3$  jets, from a combined  $Z +$  jets generation after joint generator–discriminator training.

tectures we can avoid a two-part loss functions entirely and incorporate the discriminator information into the generator loss of Eq.(6) through the event weight function  $w_D(x)$  of Eq.(12),

$$\begin{aligned} \mathcal{L}_{\text{DiscFlow}} &= \sum_{i=1}^B w_D(x_i)^\alpha \left( \frac{\psi(x_i; c_i)^2}{2} - \log J(x_i) \right) \\ &\approx \int dx \underbrace{w_D(x)^\alpha P(x)}_{\text{reweighted truth}} \left( \frac{\psi(x; c)^2}{2} - \log J(x) \right). \end{aligned} \quad (15)$$

The hyperparameter  $\alpha$  determines the impact of the discriminator weights, and we introduce an additional discriminator dependence as

$$\alpha = \alpha_0 \left| \frac{1}{2} - D(x) \right|. \quad (16)$$

Furthermore, starting at zero, we increase  $\alpha_0$  linearly during training.

From Eq.(15) we see that our modified loss is equivalent to training on a shifted reference distribution. In Fig. 6 we illustrate what happens if the generator populates a phase space region too densely and we reduce the weight of the training events there. Conversely, if a region is too sparsely populated by the generator, increased loss weights amplify the effect of the training events. Our new discriminator–generator coupling through weights has the advantage that it does not require a Nash equilibrium between two competing

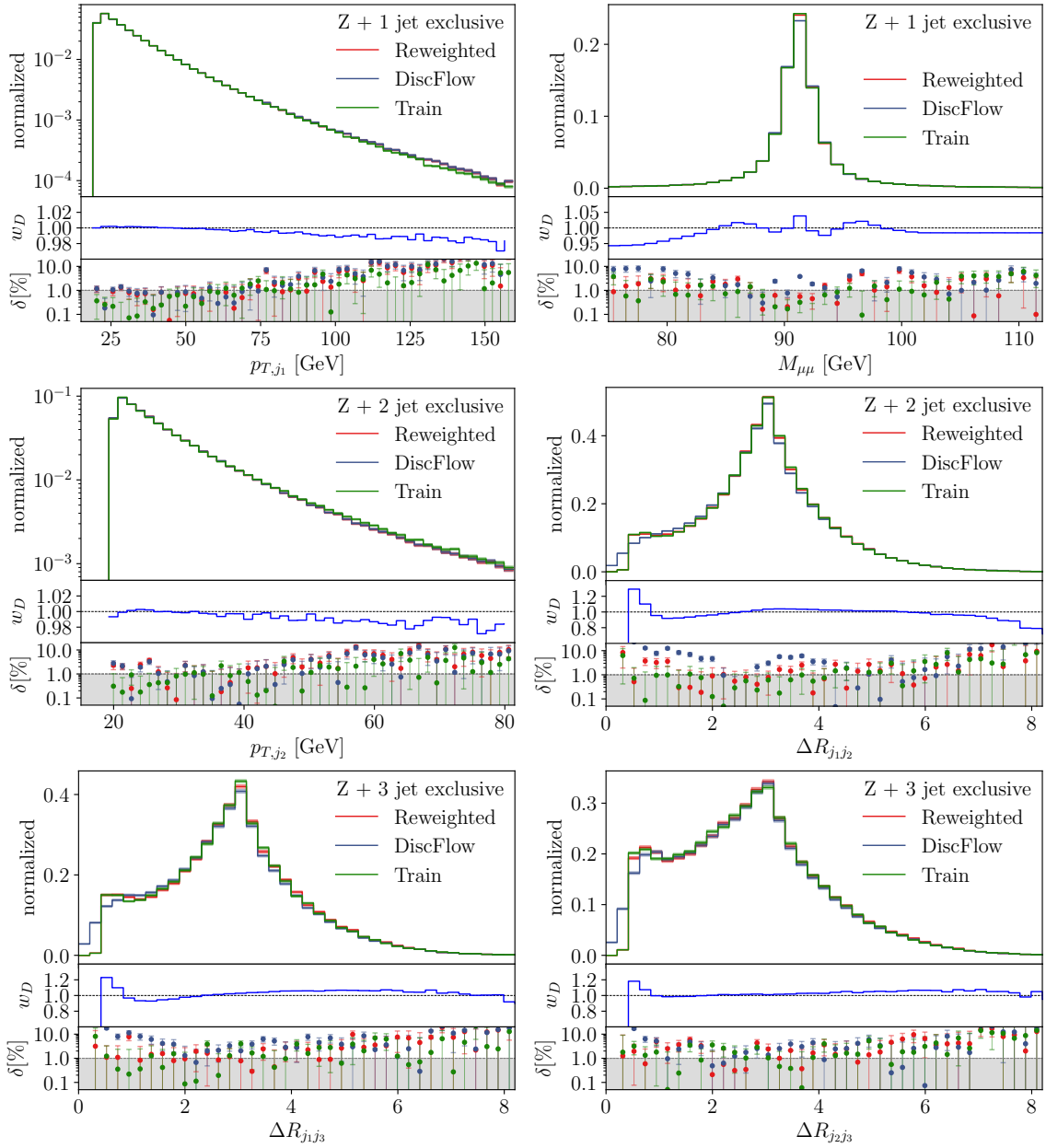


Figure 8: Discriminator-reweighted DiscFlow distributions for  $Z + 1$  jet (upper),  $Z + 2$  jets (middle), and  $Z + 3$  jets (lower) from a combined  $Z +$  jets generation. The bottom panels show the average correction factor obtained from the discriminator output, the DiscFlow results for joint generator–discriminator training and without reweighting are the same as in Fig. 7.

networks, so the discriminator can no longer overpower the generator. As the generator converges towards the true distribution, the discriminator will stabilize as  $w_D(x) \rightarrow 1$ , and the generator loss will approach its unweighted global minimum.

When training the two DiscFlow networks jointly, we split the batches per epoch equally between both networks, training each network on a separate subset of the training data. To increase the stability, we start by training the generator and the separate discriminators for the different jet multiplicities separately and only reweight the latent loss

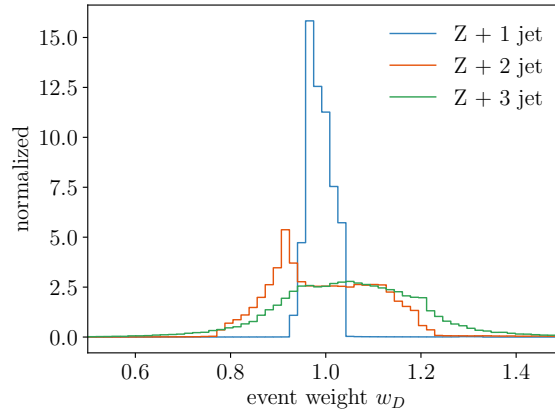


Figure 9: Distribution over the weights  $w_D$  computed over the entire, not marginalized phase space.

objective afterwards.

In Fig. 7 we show the performance of the DiscFlow setup to our  $Z$ +jets benchmark process. First, we see that in the bulk of the flat distributions like  $p_{T,j}$  the generator reproduces the correct phase space density almost at the level of the training statistics. We know that the standard INN generator fails when it comes to the precision of the  $M_{\mu\mu}$  and  $\Delta R$  distributions, and in Fig. 7 we confirm that the joint training of the generator with a discriminator corrects the invariant mass almost to the level of the training statistics. The non-negligible density of generated events below the cut at  $\Delta R = 0.4$  shows that the DiscFlow method is only effective in phase space regions populated by training data.

In the ideal AI-world we assume that after successful joint training the discriminator will have transferred all of its information into the generator, such that  $D(x) = 0.5$  at any point of phase space. In reality, this is not at all guaranteed. We know from Fig. 5 that the discriminator can learn the  $\Delta R$  features very well, so we combine the joint training and discriminator reweighting strategies to ensure that we extract the full performance of both networks. In Fig. 8 we show the same training results as in Fig. 7, but reweighted with  $w_D$ . We see that the reweighting leads to a small correction of the  $M_{\mu\mu}$ -distribution and a sizeable correction to the  $\Delta R_{jj}$  features close to the jet separation cut. Because of the way we provide the event input, we note that the transverse momentum conservation would become the next challenge after mastering  $M_{\mu\mu}$  and  $\Delta R_{jj}$ . For all other observables our reweighted DiscFlow network indeed reproduces the true kinematic distributions at the percent level provided by the training statistics.

While in Fig. 8 we see that the correction factor obtained from the discriminator shows the agreement of training events and simulated events, it is crucial that we search the fully exclusive phase space for systematic deviations between training and simulated events. In Fig. 9 we histogram all event weights  $w_D(x_i)$  for  $Z$ + jets production. For the high-statistics  $Z + 1$  jet sample the correction weights are at most at the percent level. The fact that our generator only learns the phase space density and not the total rates allows for a slight bias in the event weight distributions. For the bulk of the kinematic distributions the bin-wise correction in Fig. 8 is still slightly smaller than the weights shown here, which means that some of the corrections are simply noise. The width of the weight distribution increases for higher jet multiplicities, simply reflecting the drop in training statistics. Combining Fig. 9 and Fig. 8 allows us to trace the large weights  $w_D$  to critical phase space regions, like the lower tail of the  $M_{\mu\mu}$ -distribution for  $Z + 1$  jet or

$\Delta R_{jj} \lesssim 0.5$  for  $Z + 2/3$  jets.

## 4 Uncertainties and control

After introducing our precision generator architecture in Sec. 2 and extending it to a discriminator–generator architecture for control in Sec. 3, the last item on our list of LHC tasks is a comprehensive treatment of uncertainties. A proper uncertainty treatment has been discussed for instance for regression or classification networks [57, 58, 74], while for generative networks there exists only a first study on how to use and interpret Bayesian INNs [59]. In this final section we discuss how different uncertainties on generated events can be extracted using a Bayesian generator network, a conditional sampling using simulated uncertainties, and the discriminator introduced in the previous section. Each of these handles allows us to control certain kinds of uncertainties, and in combination they allow us to extract a meaningful uncertainty map over phase space.

### 4.1 Bayesian network

The simple idea behind Bayesian networks is to replace trained network weights by trained distributions of network weights. If we evaluate the network by sampling over these distributions, the network output will be a central value of the numerically defined function and an uncertainty distribution [53–55]. Because general MCMC-methods become expensive for larger networks, we rely on variational inference to generate the weight distributions [75]. More specifically, we rely on a Gaussian approximation for the network weight distribution and learn the mean and the standard deviation instead of just one value in a deterministic network. Because of the non-linear nature of the network the output does not have a Gaussian uncertainty distribution [58]. Our Bayesian INN (BINN) follows the same setup as our deterministic INN-generator in Sec. 2.2, converted to the Bayesian setup following Ref. [59].

For a Bayesian generative network we supplement the phase space density  $p(x)$ , encoded in the density of unweighted events, with an uncertainty map  $\sigma(x)$  over the same phase space. To extract the density we bin events in a histogram for a given observable and with finite statistics. Focussing on one histogram and omitting the corresponding phase space argument  $x$  the expected number of events per bin is

$$\langle n \rangle = \sum_n n P_N(n) , \quad (17)$$

with  $P_N(n)$  given by the binomial or Poisson probability of observing  $n$  events in this bin. This event count should be the mean of the BINN distribution, defined by sampling from the distribution  $q(\theta)$  over the network weights  $\theta$ ,

$$\langle n \rangle = \int d\theta q(\theta) \sum_n n P_N(n|\theta) \equiv \int d\theta q(\theta) \langle n \rangle_\theta . \quad (18)$$

Following the same argument as in Ref. [58] we can compute the standard deviation of

this sampled event count and split it into two terms,

$$\begin{aligned}
\sigma_{\text{tot}}^2 &= \langle (n - \langle n \rangle)^2 \rangle \\
&= \int d\theta q(\theta) [\langle n^2 \rangle_\theta - 2\langle n \rangle_\theta \langle n \rangle + \langle n \rangle^2] \\
&= \int d\theta q(\theta) [\langle n^2 \rangle_\theta - \langle n \rangle_\theta^2 + (\langle n \rangle_\theta - \langle n \rangle)^2] \equiv \sigma_{\text{stoch}}^2 + \sigma_{\text{pred}}^2 .
\end{aligned} \tag{19}$$

The first contribution to the uncertainty is the variance of the Poisson distribution,

$$\sigma_{\text{stoch}}^2 = \int d\theta q(\theta) [\langle n^2 \rangle_\theta - \langle n \rangle_\theta^2] = \langle n \rangle . \tag{20}$$

Even if the network is perfectly trained and  $q(\theta)$  turns into a delta distribution, it does not vanish, because it describes the stochastic nature of our binned data set. The second term,

$$\sigma_{\text{pred}}^2 = \int d\theta q(\theta) [\langle n \rangle_\theta - \langle n \rangle]^2 , \tag{21}$$

captures the deviation of our network from a perfectly trained network, where the widths of the network weights vanish.

Moving from a binned to a continuous distribution we can transform our results into the density and uncertainty maps over phase space, as introduced in Ref. [59]. Assuming  $\langle n \rangle \propto p(x)$ , with an appropriate proportionality factor and a continuous phase space variable  $x$ , Eqs.(18) and (21) turn into

$$\begin{aligned}
p(x) &= \int d\theta q(\theta) p(x|\theta) \\
\sigma_{\text{pred}}^2(x) &= \int d\theta q(\theta) [p(x|\theta) - p(x)]^2 .
\end{aligned} \tag{22}$$

To estimate  $\sigma_{\text{tot}}$ , we sample  $\theta$  and  $n$  from their underlying distributions and compute  $\langle n \rangle$ . In practice, we draw weights  $\theta$ , generate  $N$  events with those weights, histogram them for the observable of interest, extract  $n$  per bin. Because the INN-generator is very fast, we can repeat this process to compute the standard deviation. To see the effect of the different contributions to the BINN uncertainty we illustrate the correlation between the event count and  $\sigma_{\text{tot}}$  for  $Z + 1$  jet events, with the  $p_{T,j}$ -distribution described by 60 bins. Each of these bins corresponds to a dot in the figure. As long as our sampling is limited by the statistics of the generated events we find the expected Poisson scaling  $\sigma \propto \sqrt{\mu}$ , corresponding to the contribution  $\sigma_{\text{stoch}}$ . For larger statistics,  $\sigma_{\text{stoch}}$  becomes relatively less important, and the actual predictive uncertainty of the BINN takes over,  $\sigma_{\text{tot}} \approx \sigma_{\text{pred}}$ .

### Sources of uncertainties

By construction, Bayesian networks capture the effects of limited training statistics and non-perfect training. If we control the truth information and can augment the training data, a Bayesian network can also propagate the effects of systematic biases, systematic uncertainties, or noise into the network output [57, 58]. For generative networks, the Bayesian network is ideally suited to understand the way the network learns the phase space density by following the density map it learns in parallel [59]. As a side remark, we can use this information to track the learning of the BINN for our  $Z$ +jets events. We find

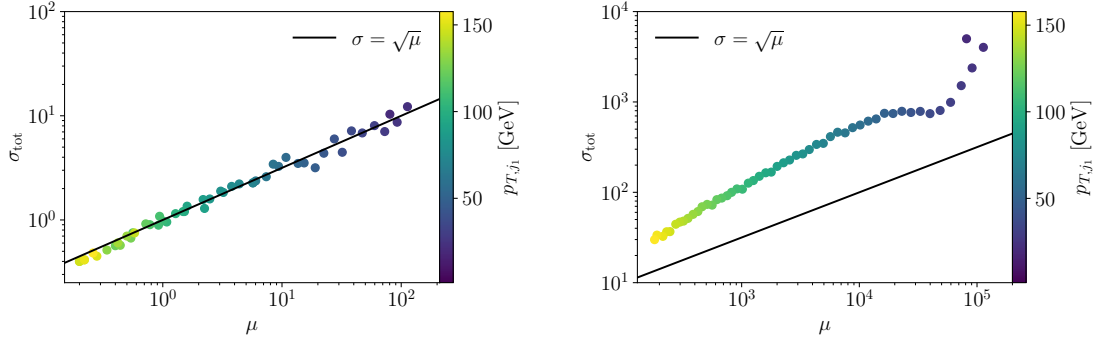


Figure 10: Correlation between event count and BINN uncertainty for 1000 (left) and 1M (right) generated events. The diagonal line defines the Gaussian scaling for a statistically limited sample.

that the network first learns the  $p_T$ -distributions of the different final-state particles quite precisely, before it targets the angular correlations. This explains why small features of the  $\Delta R$ -distributions are the hardest to learn, because they arise only for the correlation of the  $\Delta\eta$  and  $\Delta\phi$  correlations. Correspondingly, we find that one way of improving the performance on the angular correlation is to apply noise specifically to the  $p_T$ -distributions. On the other hand, the magic transformation of Eq.(8) turns out to be the more efficient solution to this problem, so we also apply it to the BINN.

When modelling different uncertainties, the problem with augmented training data for generative networks is that their training is, strictly speaking, unsupervised. We do not have access to the true density distribution and have to extract it by binning event samples. This means that additional noise will only be visible in the BINN uncertainty if it destabilizes the training altogether. Other data augmentation will simply lead to a different target density, overriding the density encoded in the original set of events. This is why in the following we will discuss training statistics and stability, and postpone the description of systematics in generative network training to Sec. 4.2.

In Fig. 11 we show the uncertainty  $\sigma_{\text{tot}} \approx \sigma_{\text{pred}}$  given by the BINN for a Bayesian version of the network introduced in Sec. 2.2, including the magic transformation for the  $\Delta R$ -distributions. As before, we see that the network learns the phase space density very precisely for simple kinematic distributions like  $p_{T,j_1}$ . The slightly worse performance compared to the deterministic network in Fig. 11 is due to the increased training effort required by the larger network. The extracted uncertainties for  $p_{T,j_1}$  and  $p_{T,j_2}$  for instance in the bulk reflect the lower statistics of the  $Z + 2$  jet training sample compared to  $Z + 1$  jet. The narrow  $M_{\mu\mu}$ -distribution challenges the uncertainty estimate in that the network learns neither the density nor the uncertainty very precisely [59]. This limitation will be overcome once the network learns the feature in the density properly. For the different  $\Delta R$ -distributions we see that the network learns the density well, thanks to the magic transformation of Eq.(8). Therefore, the network also reports a comparably large uncertainty in the critical phase space regions around  $\Delta R_{ij} = 0.4 \dots 1$ .

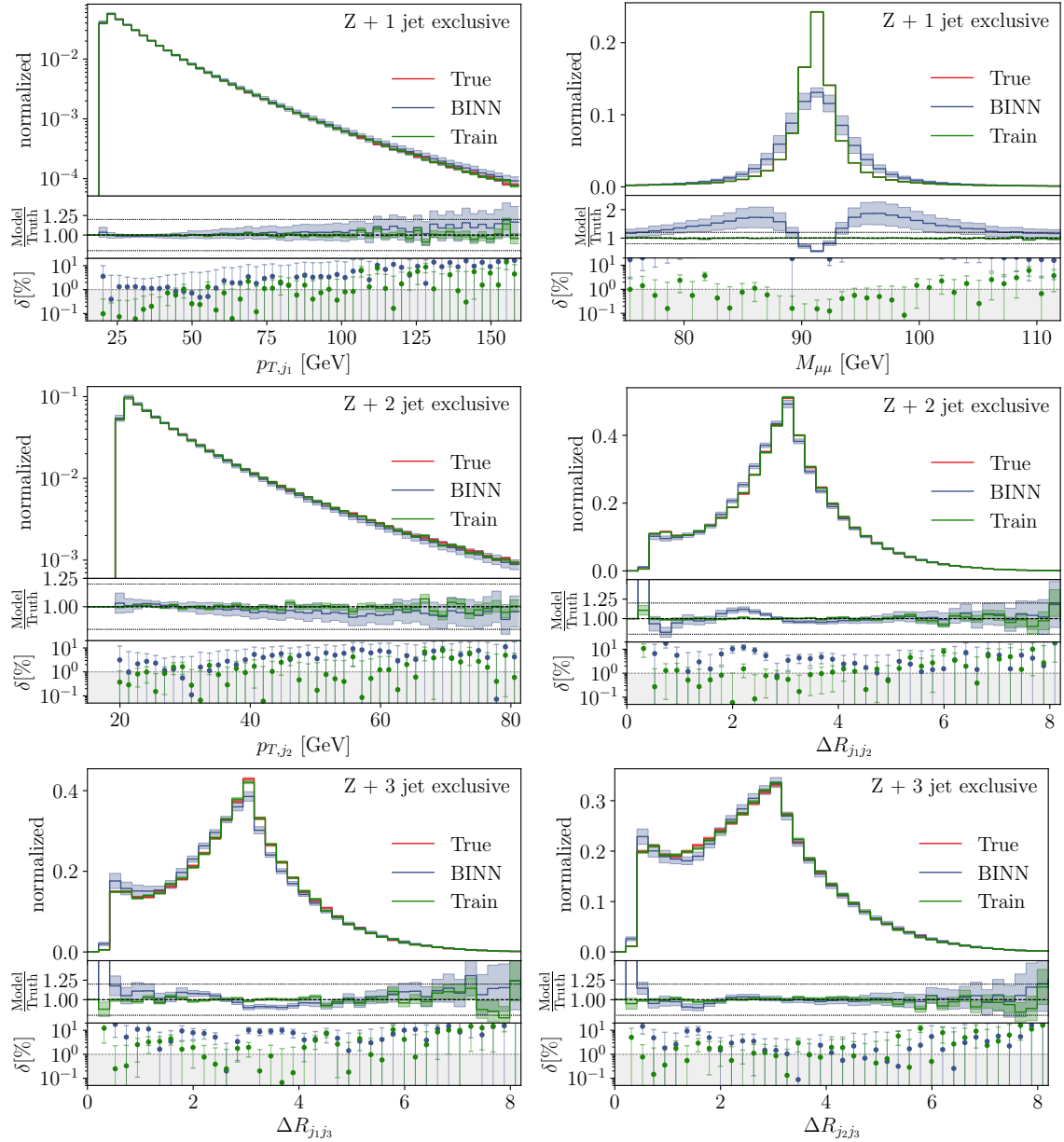


Figure 11: BINN densities and uncertainties for  $Z + 1$  jet (upper),  $Z + 2$  jets (middle), and  $Z + 3$  jets (lower) from a combined  $Z + \text{jets}$  generation. The architecture and training data correspond to the deterministic network results shown in Fig. 4, including the magic transformation of Eq.(8).

### Effect of training statistics

From the above discussion it is clear that one way to test the BINN uncertainties is to train the same network the same way, but on training samples of different size. We start with one batch size, 3072 events, and increase the training sample to the maximum of 2.7M. For  $Z + 1$  jet we show the relative uncertainty as a function of transverse momenta, for instance, in Fig. 12. In both cases we see that over most the distribution the uncertainty improves with the training statistics. However, we also see that in the low-statistics tail of  $p_{T,\mu_1}$  the low-statistics trainings systematically underestimate the uncertainty. Again, this reflects the fact that the network does not even have enough data to estimate a reasonable

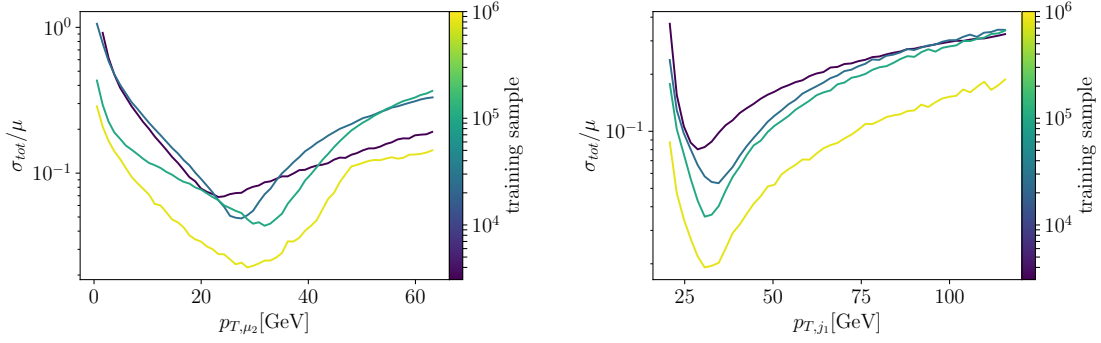


Figure 12: Relative uncertainty from the BINN for the  $Z + 1$  jet sample, as a function of the size of the training sample.

uncertainty. For  $p_{T,j1}$  this effect does not occur, even in the tails where the network has to extrapolate eventually.

## 4.2 Conditional augmentations

As discussed above, Bayesian generative networks will not capture typical systematic or theory uncertainties, because we cannot augment the input truth. Instead, we can augment our data via a nuisance parameter describing the nature and size of a systematic or theory uncertainty and train the network conditionally on this parameter. For illustration purpose, we introduce a theory uncertainty proportional to a transverse momentum scale. As a function of a nuisance parameter  $a$  we shift the unit weights in our training sample to

$$w = 1 + a \left( \frac{p_{T,j1} - 15 \text{ GeV}}{100 \text{ GeV}} \right)^2, \quad (23)$$

where the transverse momentum is given in GeV, we account for a threshold at 15 GeV, and we choose a quadratic scaling to enhance the effects of this shift in the tails.

We then train the Bayesian INN conditionally on values  $a = 0 \dots 30$  in steps of one. For the event generation incorporating the theory uncertainty we can sample kinematic distributions for different  $a$ -values. In Fig. 13 we show generated distributions for different values of  $a$ . To model the conditional parameter similar to phase space and allow for an uncertainty on the conditional nuisance parameter, we sample  $a$  with a Gaussian around its central value and a standard deviation of  $\min(a/10, 0.1)$ . The two panels show the modified  $p_{T,j1}$ -distribution and its impact on  $p_{T,j2}$  through correlations. As expected, the effects are similar, but the multi-particle recoil washes out the effects on  $p_{T,j2}$ . In the upper panels we compare the effect of the theory uncertainty  $a = 0 \dots 12$  to the statistical training uncertainty given by the BINN. We see that our method traces the additional theory or systematic uncertainty, and allows us to reliably estimate its sub-leading nature for  $p_{T,j2}$ . While we show ranges of  $a$ , corresponding to the typical flat likelihood used for theory uncertainties, we could obviously sample the different  $a$ -values during event generation. In the lower panels we show the relative BINN uncertainties, to ensure that the training for the different  $a$ -values is stable. For  $p_{T,j1}$  the data augmentation has a slight chilling effect on the high-precision training around the maximum of the distribution. In the statistically limited tails towards larger  $p_T$  the BINN training without and with augmentations behaves

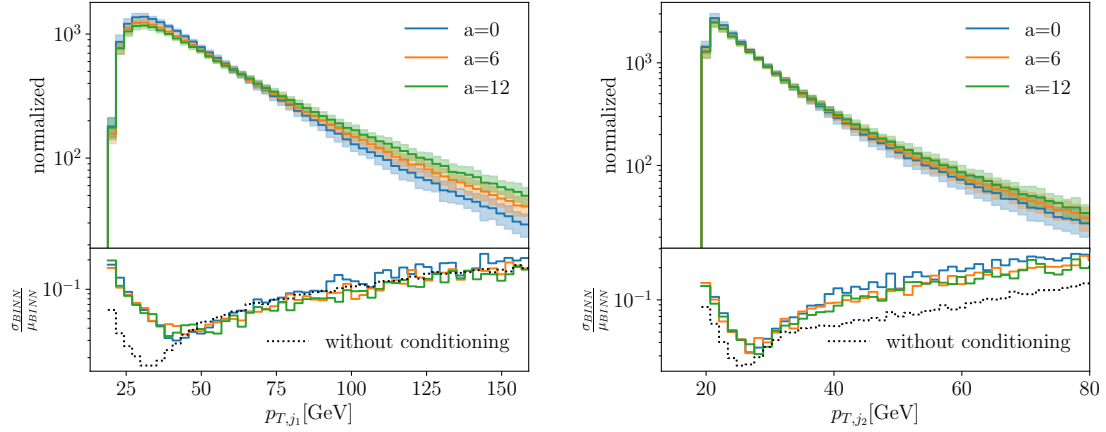


Figure 13: BINN densities for  $Z + \text{jets}$  and conditional training with an enhanced-tail augmentation in  $p_{T,1}$ , as defined in Eq.(23).

the same. Looking at the recoil correlation, the BINN reports a slightly larger uncertainty for the augmented training, correctly reflecting the fact that the network now has to learn an additional source of correlations. At least for the range of shown  $a$ -values this BINN uncertainty is independent of the size of the augmentation.

### 4.3 Discriminator for consistency

After introducing two ways of tracing specific uncertainties for generative networks and controlling their precision, we come back to the joint DiscFlow generator–discriminator training. In complete analogy to, for instance, higher-order perturbative corrections, we can use the jointly trained discriminator to improve the network precision and at the same time guide us to significant differences between training data and generated data. Because the discriminator is a simpler network than the INN-generator, it is well suited to search for deviations which the BINN misses in its density and uncertainty maps.

In Fig. 14 we illustrate the different aspects of our uncertainty-controlled precision generator. First, we see that the INN generator indeed learns and reproduces the phase space density at the level of the training statistics. In the remaining panels we show three ways to control possible uncertainty, using the discriminator, a BINN, and a BINN combined with augmented training data. Each aspect is described in detail in this paper:

- joint discriminator–generator training (DiscFlow) for precision generation — Fig. 7;
- discriminator to control inconsistencies between training and generated events — Fig. 8;
- BINN to track uncertainty on the learned phase space density — Fig. 11;
- conditional augmentation for systematic or theory uncertainties — Fig. 13.

## 5 Outlook

A crucial step in establishing generative networks as event generation tools for the LHC is the required precision in estimating the phase space density and full control of uncertainties

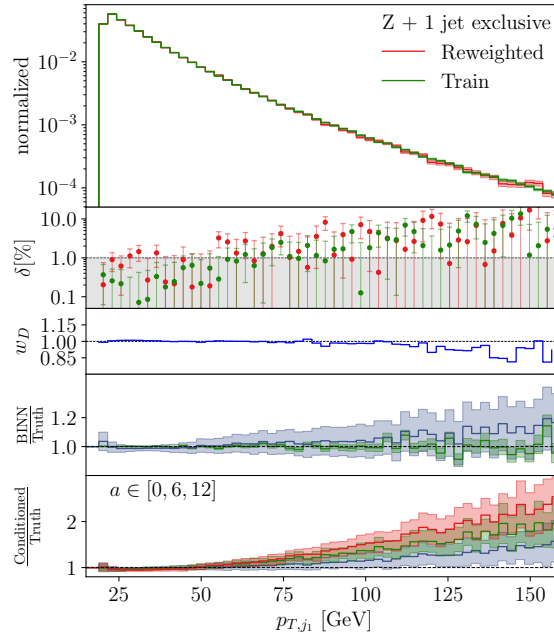


Figure 14: Illustration of uncertainty-controlled DiscFlow simulation. We show the reweighted  $p_{T,j1}$ -distribution for the inclusive  $Z$ +jets sample, combined with the discriminator  $D$ , the BINN uncertainty, and the sampled systematic uncertainty defined through the data augmentation of Eq.(23).

in generated samples.

In the first part of this paper, we have shown how INN-generators can be trained on  $Z$ +jets events with a variable number of particles in the final state, to reproduce the true phase space density at the percent level, almost on par with the statistical uncertainty of the training sample. If we are willing to work with weighted events, with event weights of order one, we can either use a magic variable transformation or an additional discriminator network to achieve high precision all over phase space. Alternatively, we can train the discriminator jointly with the generator and use our novel DiscFlow architecture to provide unweighted events with high precision (Fig. 7). This joint training does not involve a Nash equilibrium and is especially stable. Any information that the discriminator has not transferred to the generator training can eventually be included through reweighting, giving our NN-event generator high precision combined with a high level of control (Fig. 8).

In the second part of this paper we have established three methods to control the precision INN-generator and its uncertainties. First, for unsupervised generative training we can use a Bayesian INN to estimate uncertainties from limited training statistics or sub-optimal network training (Fig. 11). Second, we can augment the training data conditionally on a nuisance parameter and sample this parameter to account for systematic or theory uncertainties including the full phase space correlations (Fig. 13). A reliable estimate of the different uncertainties allows us to compare the numerical impact of the different uncertainties. Finally, we can use the jointly trained discriminator to identify phase space regions where the BINN lacks the necessary precision in its density and uncertainty maps over phase space.

All these aspects of our uncertainty-controlled precision generator are illustrated in Fig. 14. With this level of precision and control, INN-generators should be ready to be used as extremely efficient tools to generate LHC events.

## Acknowledgments

We would like to thank Michel Luchmann and Manuel Haußmann for help with Bayesian networks and Luca Mantani and Ramon Winterhalder for their work on an earlier incarnation of this project. We are also very grateful to Ulli Köthe and Lynton Ardiszone for their expert advice on many aspects of this paper. The research of AB and TP is supported by the Deutsche Forschungsgemeinschaft (DFG, German Research Foundation) under grant 396021762 – TRR 257 Particle Physics Phenomenology after the Higgs Discovery. TH is supported by the DFG Research Training Group GK-1940, Particle Physics Beyond the Standard Model. The authors acknowledge support by the state of Baden-Württemberg through bwHPC and the German Research Foundation (DFG) through grant no INST 39/963-1 FUGG (bwForCluster NEMO).

## References

- [1] A. Butter and T. Plehn, *Generative Networks for LHC events*, arXiv:2008.08558 [hep-ph].
- [2] I. J. Goodfellow, J. Pouget-Abadie, M. Mirza, B. Xu, D. Warde-Farley, S. Ozair, A. Courville, and Y. Bengio, *Generative adversarial networks*, arXiv:1406.2661 [stat.ML].
- [3] A. Creswell, T. White, V. Dumoulin, K. Arulkumaran, B. Sengupta, and A. A. Bharath, *Generative adversarial networks: An overview*, IEEE Signal Processing Magazine **35** (Jan, 2018) 53–65.
- [4] A. Butter, S. Diefenbacher, G. Kasieczka, B. Nachman, and T. Plehn, *GANplifying event samples*, SciPost Phys. **10** (2021) 6, 139, arXiv:2008.06545 [hep-ph].
- [5] D. P. Kingma and M. Welling, *Auto-encoding variational bayes*, arXiv:1312.6114 [stat.ML].
- [6] D. P. Kingma and M. Welling, *An introduction to variational autoencoders*, Foundations and Trends® in Machine Learning **12** (2019) 4, 307–392.
- [7] D. Rezende and S. Mohamed, *Variational inference with normalizing flows*, in *Proceedings of the 32nd International Conference on Machine Learning*, F. Bach and D. Blei, eds. PMLR, Lille, France, 07–09 Jul, 2015. arXiv:1505.05770 [stat.ML].
- [8] I. Kobyzev, S. Prince, and M. Brubaker, *Normalizing flows: An introduction and review of current methods*, IEEE Transactions on Pattern Analysis and Machine Intelligence (2020) 1–1.
- [9] G. Papamakarios, E. Nalisnick, D. J. Rezende, S. Mohamed, and B. Lakshminarayanan, *Normalizing flows for probabilistic modeling and inference*, arXiv:1912.02762 [stat.ML].
- [10] I. Kobyzev, S. Prince, and M. A. Brubaker, *Normalizing flows: An introduction and review of current methods*, arXiv:1908.09257 [stat.ML].
- [11] T. Müller, B. McWilliams, F. Rousselle, M. Gross, and J. Novák, *Neural importance sampling*, arXiv:1808.03856 [cs.LG].

- [12] L. Ardizzone, J. Kruse, S. Wirkert, D. Rahner, E. W. Pellegrini, R. S. Klessen, L. Maier-Hein, C. Rother, and U. Köthe, *Analyzing inverse problems with invertible neural networks*, arXiv:1808.04730 [cs.LG].
- [13] L. Dinh, J. Sohl-Dickstein, and S. Bengio, *Density estimation using real nvp*, arXiv:1605.08803 [cs.LG].
- [14] D. P. Kingma and P. Dhariwal, *Glow: Generative flow with invertible 1x1 convolutions*, arXiv:1807.03039 [stat.ML].
- [15] M. D. Klimek and M. Perelstein, *Neural Network-Based Approach to Phase Space Integration*, arXiv:1810.11509 [hep-ph].
- [16] I.-K. Chen, M. D. Klimek, and M. Perelstein, *Improved Neural Network Monte Carlo Simulation*, SciPost Phys. **10** (2021) 023, arXiv:2009.07819 [hep-ph].
- [17] E. Bothmann, T. Janßen, M. Knobbe, T. Schmale, and S. Schumann, *Exploring phase space with Neural Importance Sampling*, SciPost Phys. **8** (2020) 4, 069, arXiv:2001.05478 [hep-ph].
- [18] C. Gao, J. Isaacson, and C. Krause, *i-flow: High-dimensional Integration and Sampling with Normalizing Flows*, Mach. Learn. Sci. Tech. **1** (2020) 4, 045023, arXiv:2001.05486 [physics.comp-ph].
- [19] C. Gao, S. Höche, J. Isaacson, C. Krause, and H. Schulz, *Event Generation with Normalizing Flows*, Phys. Rev. D **101** (2020) 7, 076002, arXiv:2001.10028 [hep-ph].
- [20] K. Danziger, T. Janßen, S. Schumann, and F. Siegert, *Accelerating Monte Carlo event generation – rejection sampling using neural network event-weight estimates*, arXiv:2109.11964 [hep-ph].
- [21] F. Bishara and M. Montull, *(Machine) Learning Amplitudes for Faster Event Generation*, arXiv:1912.11055 [hep-ph].
- [22] S. Badger and J. Bullock, *Using neural networks for efficient evaluation of high multiplicity scattering amplitudes*, JHEP **06** (2020) 114, arXiv:2002.07516 [hep-ph].
- [23] A. Butter, T. Plehn, and R. Winterhalder, *How to GAN Event Subtraction*, SciPost Phys. Core **3** (2020) 009, arXiv:1912.08824 [hep-ph].
- [24] B. Stienen and R. Verheyen, *Phase Space Sampling and Inference from Weighted Events with Autoregressive Flows*, SciPost Phys. **10** (2021) 038, arXiv:2011.13445 [hep-ph].
- [25] M. Backes, A. Butter, T. Plehn, and R. Winterhalder, *How to GAN Event Unweighting*, SciPost Phys. **10** (2021) 4, 089, arXiv:2012.07873 [hep-ph].
- [26] E. Bothmann and L. Debbio, *Reweighting a parton shower using a neural network: the final-state case*, JHEP **01** (2019) 033, arXiv:1808.07802 [hep-ph].
- [27] L. de Oliveira, M. Paganini, and B. Nachman, *Learning Particle Physics by Example: Location-Aware Generative Adversarial Networks for Physics Synthesis*, Comput. Softw. Big Sci. **1** (2017) 1, 4, arXiv:1701.05927 [stat.ML].
- [28] J. W. Monk, *Deep Learning as a Parton Shower*, JHEP **12** (2018) 021, arXiv:1807.03685 [hep-ph].

- [29] A. Andreassen, I. Feige, C. Frye, and M. D. Schwartz, *JUNIPR: a Framework for Unsupervised Machine Learning in Particle Physics*, Eur. Phys. J. **C79** (2019) 2, 102, arXiv:1804.09720 [hep-ph].
- [30] K. Dohi, *Variational Autoencoders for Jet Simulation*, arXiv:2009.04842 [hep-ph].
- [31] F. A. Di Bello, S. Ganguly, E. Gross, M. Kado, M. Pitt, L. Santi, and J. Shlomi, *Towards a Computer Vision Particle Flow*, Eur. Phys. J. C **81** (2021) 2, 107, arXiv:2003.08863 [physics.data-an].
- [32] P. Baldi, L. Blecher, A. Butter, J. Collado, J. N. Howard, F. Keilbach, T. Plehn, G. Kasieczka, and D. Whiteson, *How to GAN Higher Jet Resolution*, arXiv:2012.11944 [hep-ph].
- [33] S. Otten, S. Caron, W. de Swart, M. van Beekveld, L. Hendriks, C. van Leeuwen, D. Podareanu, R. Ruiz de Austri, and R. Verheyen, *Event Generation and Statistical Sampling for Physics with Deep Generative Models and a Density Information Buffer*, Nature Commun. **12** (2021) 1, 2985, arXiv:1901.00875 [hep-ph].
- [34] B. Hashemi, N. Amin, K. Datta, D. Olivito, and M. Pierini, *LHC analysis-specific datasets with Generative Adversarial Networks*, arXiv:1901.05282 [hep-ex].
- [35] R. Di Sipio, M. Faucci Giannelli, S. Ketabchi Haghighat, and S. Palazzo, *DijetGAN: A Generative-Adversarial Network Approach for the Simulation of QCD Dijet Events at the LHC*, JHEP **08** (2020) 110, arXiv:1903.02433 [hep-ex].
- [36] A. Butter, T. Plehn, and R. Winterhalder, *How to GAN LHC Events*, SciPost Phys. **7** (2019) 6, 075, arXiv:1907.03764 [hep-ph].
- [37] Y. Alanazi, N. Sato, T. Liu, W. Melnitchouk, M. P. Kuchera, E. Pritchard, M. Robertson, R. Strauss, L. Velasco, and Y. Li, *Simulation of electron-proton scattering events by a Feature-Augmented and Transformed Generative Adversarial Network (FAT-GAN)*, arXiv:2001.11103 [hep-ph].
- [38] M. Paganini, L. de Oliveira, and B. Nachman, *Accelerating Science with Generative Adversarial Networks: An Application to 3D Particle Showers in Multilayer Calorimeters*, Phys. Rev. Lett. **120** (2018) 4, 042003, arXiv:1705.02355 [hep-ex].
- [39] M. Paganini, L. de Oliveira, and B. Nachman, *CaloGAN : Simulating 3D high energy particle showers in multilayer electromagnetic calorimeters with generative adversarial networks*, Phys. Rev. **D97** (2018) 1, 014021, arXiv:1712.10321 [hep-ex].
- [40] P. Musella and F. Pandolfi, *Fast and Accurate Simulation of Particle Detectors Using Generative Adversarial Networks*, Comput. Softw. Big Sci. **2** (2018) 1, 8, arXiv:1805.00850 [hep-ex].
- [41] M. Erdmann, L. Geiger, J. Glombitza, and D. Schmidt, *Generating and refining particle detector simulations using the Wasserstein distance in adversarial networks*, Comput. Softw. Big Sci. **2** (2018) 1, 4, arXiv:1802.03325 [astro-ph.IM].
- [42] M. Erdmann, J. Glombitza, and T. Quast, *Precise simulation of electromagnetic calorimeter showers using a Wasserstein Generative Adversarial Network*, Comput. Softw. Big Sci. **3** (2019) 4, arXiv:1807.01954 [physics.ins-det].

- [43] ATLAS Collaboration, “Energy resolution with a GAN for Fast Shower Simulation in ATLAS.” ATLAS-SIM-2019-004, 2019.  
<https://atlas.web.cern.ch/Atlas/GROUPS/PHYSICS/PLOTS/SIM-2019-004/>.
- [44] D. Belayneh *et al.*, *Calorimetry with Deep Learning: Particle Simulation and Reconstruction for Collider Physics*, Eur. Phys. J. C **80** (2020) 7, 688, arXiv:1912.06794 [physics.ins-det].
- [45] E. Buhmann, S. Diefenbacher, E. Eren, F. Gaede, G. Kasieczka, A. Korol, and K. Krüger, *Getting High: High Fidelity Simulation of High Granularity Calorimeters with High Speed*, Comput. Softw. Big Sci. **5** (2021) 1, 13, arXiv:2005.05334 [physics.ins-det].
- [46] E. Buhmann, S. Diefenbacher, E. Eren, F. Gaede, G. Kasieczka, A. Korol, and K. Krüger, *Decoding Photons: Physics in the Latent Space of a BIB-AE Generative Network*, arXiv:2102.12491 [physics.ins-det].
- [47] C. Chen, O. Cerri, T. Q. Nguyen, J. R. Vlimant, and M. Pierini, *Analysis-Specific Fast Simulation at the LHC with Deep Learning*, Comput. Softw. Big Sci. **5** (2021) 1, 15.
- [48] C. Krause and D. Shih, *CaloFlow: Fast and Accurate Generation of Calorimeter Showers with Normalizing Flows*, arXiv:2106.05285 [physics.ins-det].
- [49] K. Datta, D. Kar, and D. Roy, *Unfolding with Generative Adversarial Networks*, arXiv:1806.00433 [physics.data-an].
- [50] M. Bellagente, A. Butter, G. Kasieczka, T. Plehn, and R. Winterhalder, *How to GAN away Detector Effects*, SciPost Phys. **8** (2020) 4, 070, arXiv:1912.00477 [hep-ph].
- [51] M. Bellagente, A. Butter, G. Kasieczka, T. Plehn, A. Rousselot, R. Winterhalder, L. Ardizzone, and U. Köthe, *Invertible Networks or Partons to Detector and Back Again*, SciPost Phys. **9** (2020) 074, arXiv:2006.06685 [hep-ph].
- [52] S. Bieringer, A. Butter, T. Heimel, S. Höche, U. Köthe, T. Plehn, and S. T. Radev, *Measuring QCD Splittings with Invertible Networks*, SciPost Phys. **10** (2021) 6, 126, arXiv:2012.09873 [hep-ph].
- [53] D. MacKay, *Probable Networks and Plausible Predictions – A Review of Practical Bayesian Methods for Supervised Neural Networks*, Comp. in Neural Systems **6** (1995) 4679.
- [54] R. M. Neal, *Bayesian learning for neural networks*. PhD thesis, Toronto, 1995.
- [55] Y. Gal, *Uncertainty in Deep Learning*. PhD thesis, Cambridge, 2016.
- [56] A. Kendall and Y. Gal, *What Uncertainties Do We Need in Bayesian Deep Learning for Computer Vision?*, Proc. NIPS (2017) , arXiv:1703.04977 [cs.CV].
- [57] S. Bollweg, M. Haußmann, G. Kasieczka, M. Luchmann, T. Plehn, and J. Thompson, *Deep-Learning Jets with Uncertainties and More*, SciPost Phys. **8** (2020) 1, 006, arXiv:1904.10004 [hep-ph].
- [58] G. Kasieczka, M. Luchmann, F. Otterpohl, and T. Plehn, *Per-Object Systematics using Deep-Learned Calibration*, SciPost Phys. **9** (2020) 089, arXiv:2003.11099 [hep-ph].

- [59] M. Bellagente, M. Haußmann, M. Luchmann, and T. Plehn, *Understanding Event-Generation Networks via Uncertainties*, arXiv:2104.04543 [hep-ph].
- [60] Sherpa, E. Bothmann *et al.*, *Event Generation with Sherpa 2.2*, SciPost Phys. **7** (2019) 3, 034, arXiv:1905.09127 [hep-ph].
- [61] S. Catani, F. Krauss, R. Kuhn, and B. R. Webber, *QCD matrix elements + parton showers*, JHEP **11** (2001) 063, arXiv:hep-ph/0109231.
- [62] M. Cacciari, G. P. Salam, and G. Soyez, *FastJet User Manual*, Eur. Phys. J. C **72** (2012) 1896, arXiv:1111.6097 [hep-ph].
- [63] M. Cacciari, G. P. Salam, and G. Soyez, *The anti- $k_t$  jet clustering algorithm*, JHEP **04** (2008) 063, arXiv:0802.1189 [hep-ph].
- [64] A. Paszke, S. Gross, F. Massa, A. Lerer, J. Bradbury, G. Chanan, T. Killeen, Z. Lin, N. Gimelshein, L. Antiga, A. Desmaison, A. Kopf, E. Yang, Z. DeVito, M. Raison, A. Tejani, S. Chilamkurthy, B. Steiner, L. Fang, J. Bai, and S. Chintala, *Pytorch: An imperative style, high-performance deep learning library*, in *Advances in Neural Information Processing Systems 32*, H. Wallach, H. Larochelle, A. Beygelzimer, F. d'Alché Buc, E. Fox, and R. Garnett, eds., pp. 8024–8035. Curran Associates, Inc., 2019. arXiv:1912.01703 [cs.LG].
- [65] D. P. Kingma and J. Ba, *Adam: A Method for Stochastic Optimization*, arXiv:1412.6980 [cs.LG].
- [66] L. N. Smith and N. Topin, *Super-convergence: Very fast training of neural networks using large learning rates*, in *Artificial Intelligence and Machine Learning for Multi-Domain Operations Applications*, International Society for Optics and Photonics. 2019.
- [67] L. Ardizzone, C. Lüth, J. Kruse, C. Rother, and U. Köthe, *Guided image generation with conditional invertible neural networks*, arXiv:1907.02392 [cs.CV].
- [68] C. Durkan, A. Bekasov, I. Murray, and G. Papamakarios, *Cubic-spline flows*, arXiv preprint arXiv:1906.02145 (2019) .
- [69] R. Winterhalder, M. Bellagente, and B. Nachman, *Latent Space Refinement for Deep Generative Models*, arXiv:2106.00792 [stat.ML].
- [70] M. Erdmann, L. Geiger, J. Glombitza, and D. Schmidt, *Generating and refining particle detector simulations using the Wasserstein distance in adversarial networks*, Comput. Softw. Big Sci. **2** (2018) 1, 4, arXiv:1802.03325 [astro-ph.IM].
- [71] S. Diefenbacher, E. Eren, G. Kasieczka, A. Korol, B. Nachman, and D. Shih, *DCTRGAN: Improving the Precision of Generative Models with Reweighting*, JINST **15** (2020) 11, P11004, arXiv:2009.03796 [hep-ph].
- [72] I. J. Goodfellow, J. Pouget-Abadie, M. Mirza, B. Xu, D. Warde-Farley, S. Ozair, A. Courville, and Y. Bengio, *Generative adversarial nets*, in *Proceedings of the 27th International Conference on Neural Information Processing Systems - Volume 2*, NIPS'14. MIT Press, Cambridge, MA, USA, 2014.
- [73] A. Grover, M. Dhar, and S. Ermon, *Flow-gan: Combining maximum likelihood and adversarial learning in generative models*, in *AAAI Conference on Artificial Intelligence*. 2018.

- [74] B. Nachman, *A guide for deploying Deep Learning in LHC searches: How to achieve optimality and account for uncertainty*, SciPost Phys. **8** (2020) 090, arXiv:1909.03081 [hep-ph].
- [75] D. M. Blei, A. Kucukelbir, and J. D. McAuliffe, *Variational inference: A review for statisticians*, Journal of the American statistical Association **112** (2017) 518, 859.